Applied Physics Letters

Zero-phase propagation in realistic plate-type acoustic metamaterials

Cite as: Appl. Phys. Lett. **115**, 134101 (2019); https://doi.org/10.1063/1.5121295
Submitted: 23 July 2019 . Accepted: 05 September 2019 . Published Online: 23 September 2019

M. Malléjac, A. Merkel, J. Sánchez-Dehesa, J. Christensen, V. Tournat, J.-P. Groby, and V. Romero-García

Applied Physics Letters ARTICLE scitation.org/journal/apl

Zero-phase propagation in realistic plate-type acoustic metamaterials

Cite as: Appl. Phys. Lett. **115**, 134101 (2019); doi: 10.1063/1.5121295
Submitted: 23 July 2019 · Accepted: 5 September 2019 ·
Published Online: 23 September 2019

View Online Export Citation CrossMark

M. Malléjac,[1,a] A. Merkel,[2,b] J. Sánchez-Dehesa,[3] J. Christensen,[2] V. Tournat,[1] J.-P. Groby,[1] and V. Romero-García[1]

AFFILIATIONS

[1]Laboratoire d'Acoustique de l'Université du Mans, LAUM-UMR 6613 CNRS, Le Mans Université, Avenue Olivier Messiaen, 72085 Le Mans Cedex 9, France
[2]Department of Physics, Universidad Carlos III de Madrid, Avenida de la Universidad, 28911 Leganés (Madrid), Spain
[3]Wave Phenomena Group, Department of Electronic Engineering, Universitat Politècnica de València, Camino de Vera s/n, ES-46022 València, Spain

[a]**Electronic mail:** matthieu.mallejac@univ-lemans.fr
[b]**Present address:** Institut Jean Lamour, Université de Lorraine, CNRS, F-54000 Nancy, France.

ABSTRACT

We theoretically, numerically, and experimentally analyze the Density-Near-Zero (DNZ) regime of a one-dimensional acoustic metamaterial. This acoustic metamaterial is composed of thin elastic plates periodically clamped in an air-filled waveguide, and the effective dynamic zero mass density is obtained from the strong dispersion around the bandgaps associated with the resonances of the plates. We emphasize the importance of the impedance mismatch between the acoustic metamaterial and the surrounding waveguide at the frequency of the zero effective density in addition to the consequences of the inherent losses. As a result, the frequency of the zero phase propagation, i.e., the acoustic propagation with zero phase delay, is not exactly the frequency of the zero density and lies in the frequency bandgap where the effective density is negative. Considering these limitations, the zero phase propagation is still experimentally observed and a subwavelength acoustic dipole is numerically designed, thus demonstrating the possible realistic implementations of DNZ acoustic metamaterials.

Acoustic and elastic metamaterials have attracted considerable attention in the last few decades,[1–4] certainly fueled by the possibilities of tailoring their wave-dispersion properties and making previously unexpected behaviors real. Actually, a plethora of effective dynamic mass density values can be achieved, from negative[5–8] to positive mass density, thus presenting a zero mass density at specific frequency. At the frequency at which the material mass density vanishes, the supported acoustic waves present a phase velocity tending to infinity in the lossless case, leading to an effective quasistatic field distribution[9–11] or, equivalently, to an infinite wavelength. In light of these features, some outstanding effects and applications were initially proposed in electromagnetics and optics by using the epsilon near zero metamaterials. Radiation patterning and lensing[12] or energy super-squeezing and tunneling via narrow ducts are examples of these possibilities.[13–16] In acoustics, extraordinary properties have been numerically predicted based on Density-Near-Zero (DNZ) lossless metamaterials, like extraordinary sound transmission through ultranarrow channels[17] and unity transmission through sharp bends and perfect power dividers.[18] The geometric mismatch between a large cross-sectional air-filled waveguide and this ultranarrow channel is perfectly compensated by the extremely low density of the material occupying the channel, thus realizing a perfect impedance matching and an extraordinary tunneling via a supercoupling effect. This effect is accompanied by a large and uniform field enhancement along the channel and a zero-phase propagation of the wave front from the input to the output of the waveguide, implying a quasistatic wave propagation due to the extremely low value of the density. It is worth noting here that the mass density should not be zero, since it would imply an infinite impedance mismatch, but its value needs to be in the near zero region in order to compensate the cross section drop. Therefore, in the ultranarrow channels with DNZ metamaterials, the impedance matching and the wave tunneling do not depend on the channel length nor on the presence of bends, twists, and even absorbing sections along the channel. Supercoupling is thus ideal for long-distant waveguide coupling with a high transmittance and no phase delay,[17,19] light concentration and harvesting,[13,14,20] sensing,[21] filtering,[9] and nonlinear

applications.[22,23] In the absence of huge cross-sectional change, the impedance matching should be achieved when the bulk modulus is nearly infinite.[24]

A DNZ material can be made using different systems including plate-type acoustic metamaterials[7,17,25,26] or periodic distributions of structured cylindrical scatterers embedded in two-dimensional waveguides.[18] On the one hand, plate type acoustic metamaterials[2,3] are of great practical interest thanks to their huge tunability. In particular, structured arrays of such elastic elements allow us to break the density law and thus make them good candidates for achieving DNZ metamaterials.[7,17,25] However, wave energy losses, not avoidable in this kind of system,[27–29] can dramatically alter its dispersion properties and as a consequence drastically affect the DNZ metamaterial behavior. When plate-type materials are considered, the viscoelasticity of the plate material in the ultranarrow tube influences the DNZ transmission peak amplitude.[17] Low damping viscoelastic plate material has thus to be selected. On the other hand, when periodic distributions of structured cylindrical scatterers embedded in a two-dimensional waveguide are considered, impedance matching is fulfilled in the double negativity regime, which is reached over a narrow frequency band. However, these systems are not able to maintain the extraordinary features associated with double negativity because of the viscothermal losses[29] which are inherent to the system geometry.

In this work, we show that zero phase propagation can be achieved in a Plate-type Acoustic Metamaterial (PAM) and can be a promising tool for directive acoustic emission or wavefront shaping devices. The unit cell of length L_{unit} forming the PAM is shown in Fig. 1 and is composed of one plate of thickness $h = 102\,\mu$m and radius $R = 1.615$ cm which is surrounded on both sides by two cylindrical cavities of length $L_{gap}/2$ giving $L_{unit} = L_{gap} + h$. The inner and outer radii of the cylinders, which are made of aluminum, are $R_i = 1.5$ cm and $R_o = 1.615$, respectively. The plate is clamped between the two aluminum cylinders using 500 μm thick annular Teflon rings in order to enhance the reproducibility of the clamped condition. N unit cells are then hold together in a sample holder, and a uniform pressure is applied on the sample by screws at the extremities.

The elastic parameters characterizing the plates are extracted from the experimental results [see supplementary material (S.III)]. These parameters are the complex Young's Modulus $E = E_0(1 + i\beta)$, which contains the elastic part $E_0 = 4.6$ GPa and the loss factor $\beta = 0.13$ to account for the viscoelastic losses, Poisson's ratio $\nu = 0.4$, and the mass density $\rho = 1400\,\mathrm{kg\,m^{-3}}$. The plastic shim constituting the plates is chosen for its low loss factor. The resonance frequency of one single plate is experimentally measured at $f_m = 438$ Hz which gives in the lossless case $f_m = 423$ Hz. In the cylindrical cavities surrounding the plates, the viscothermal losses are accounted for by considering a complex wavenumber $k_0(\omega)$ and an impedance $Z_0(\omega)$,[30,31] where ω is the cyclic frequency.

The theoretical effective dynamic mass density $\rho(\omega)$ of an infinite lossless PAM is first analyzed and paralleled up with the transmission and reflection coefficients of a PAM of finite size composed of $N = 1$, 3, 6, and 9 unit cells as shown in Fig. 2. The effective mass density is found with $\rho(\omega) = Z(\omega)/c(\omega)$, where $c(\omega) = \omega/k(\omega)$ is the effective sound velocity and $k(\omega)$ and $Z(\omega)$ are the effective wavenumber and impedance of the PAM, respectively. The effective frequency dependent wavenumber $k(\omega)$ and impedance $Z(\omega)$ of the PAM are obtained from the transfer matrix of a single unit cell as follows:

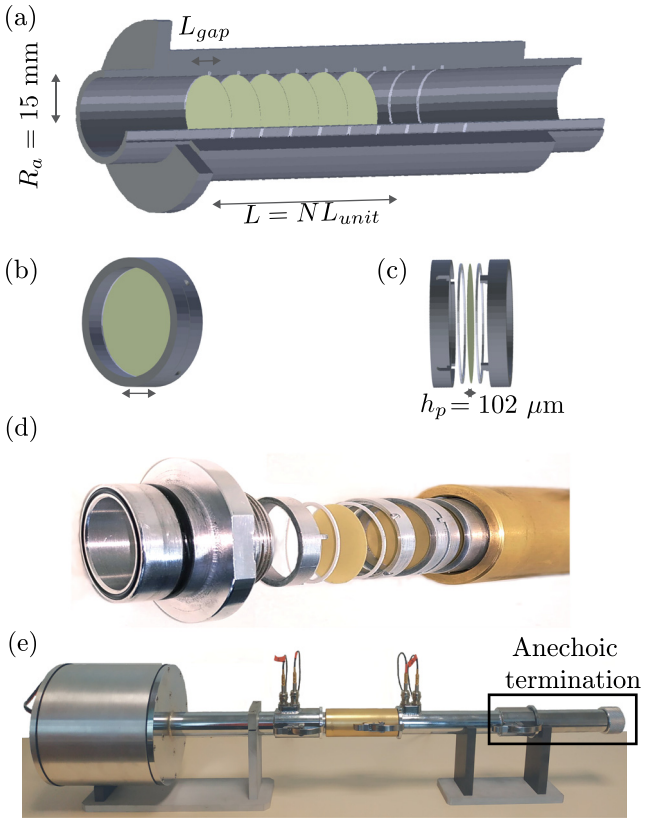

FIG. 1. (a) Considered plate-based metamaterial sketch, [(b) and (c)] unit cell, (d) photography of an exploded view of the unit cell composed of a thin elastic plate embedded between two Teflon and aluminum rings, and (e) photography of the experimental setup.

$$k(\omega)L_{unit} = \cos^{-1}[(T_{11} + T_{22})/2], \tag{1}$$

$$Z(\omega) = (T_{12}/T_{21})^{\frac{1}{2}}, \tag{2}$$

where T_{ij} are the ij-th element of the 2×2 transfer matrix which is obtained theoretically [see supplementary material (S.I)] and can be extracted from the experimental and numerical scattering coefficients.

We define three characteristic frequencies.

The first one is the resonance frequency of the plate, f_m, where the PAM impedance matches that of the air. At f_m, perfect transmission is achieved, because of the impedance matching condition, with a phase shift related to the length $L = NL_{unit}$ of the material. The phase equals the one produced in an air-filled cavity of the same length. The second frequency of interest is that at which the dynamic mass density reaches the zero value f_{ρ_0}. At this particular frequency, zero-phase delay propagation and a constant wavefield within the PAM are expected, but the PAM is not impedance matched with the surrounding medium. The amplitude of the transmission coefficient is thus not unitary and more importantly depends on the number N of unit cells. The phase shift at f_{ρ_0} is weaker than that at f_m (when the system is impedance matched), but even more importantly, it depends on N. Therefore, no propagation without phase change is supported by the system at f_{ρ_0}. The third important frequency is that at which the phase

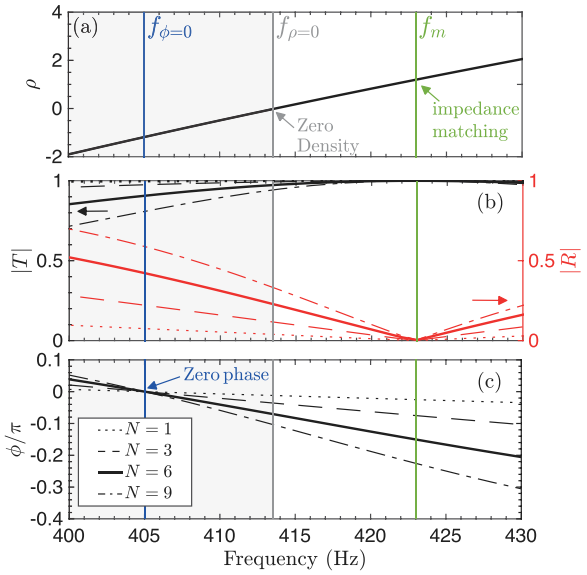

FIG. 2. Effective mass density and scattering properties of the PAM in the lossless case. (a) Effective dynamic mass density in terms of function as obtained from Eqs. (1) and (2). (b) and (c) represent the amplitude of the transmission [left vertical axis of (b)] and reflection [right vertical axis of (b)] coefficients as well as the normalized phase of the transmission coefficient for a finite PAM made of $N = 1$, 3, 6, and 9 plates, respectively. Vertical blue, gray, and green lines in (a), (b), and (c) represent the frequencies for the zero phase, $f_{\phi=0}$, zero mass density, $f_{\rho=0}$, and impedance matching, f_m, frequencies, respectively. The gray mapped area delimits the zero-frequency bandgap of an infinite system.

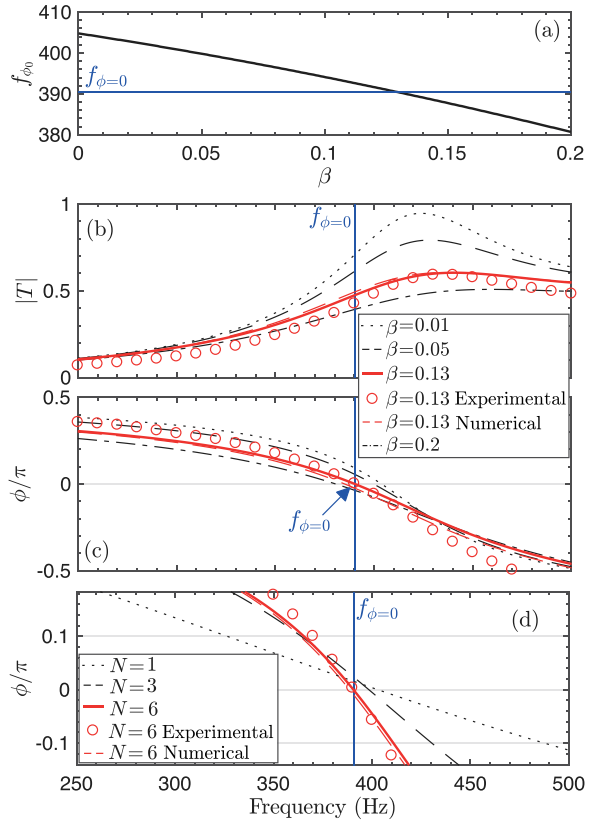

FIG. 3. Analysis of the zero phase frequency and the scattering properties of the PAM considering the viscoelastic and viscothermal losses. (a) Dependence of the zero phase frequency on the viscoelastic losses of the system. (b) and (c) represent the amplitude of the transmission coefficient as well as its normalized phase for a finite PAM made of $N = 6$ plates depending on the losses. (d) represents the dependence of the phase of the transmission coefficient with the number of unit cells in the PAM for the case with $\beta = 0.13$ (experimental losses). Continuous lines, dashed lines, and symbols in (b)–(d) represent the experimental, numerical, and analytical results, respectively. Horizontal and vertical blue lines in (a)–(d) represent the frequency for the zero phase PAM experimentally analyzed in this work.

of the transmission coefficient is exactly zero $f_{\phi=0}$. At this frequency, the effective density is negative and equal to $\rho(\omega) = -\rho_0\kappa_0/\kappa(\omega)$ [see supplementary material (S.V)]. The negative effective density regime [gray mapped areas in Fig. 2(c)] corresponds to a stop band for an infinite system. Although $f_{\phi=0}$ lies in the negative mass range, the transmission remains considerable due to the small size of the considered PAM. The amplitude of the transmission coefficient also depends on the number of unit cells composing the system, but the zero phase propagation is operated independently of the number of unit cells. Having zero density, zero phase, and unitary transmission at the exact same frequency would also imply to have an infinite bulk modulus [see supplementary material (S.V)], which is not the case in the PAM.

We now analyze the limits of zero phase transmission in the presence of losses when $N \leq 6$. These numbers of unit cells constitute a good balance between the finite size of the system and the transmission coefficient amplitude value in the lossless case at $f_{\phi=0}$ ($|T| \geq 0.9$). Both viscothermal losses in the waveguide and viscoelasticity of the plate material are accounted for. First, we analyze the dependence of the zero phase frequency, $f_{\phi=0}$, on the viscoelastic losses which are the most important loss source in usual PAM. The zero phase frequency decreases with the increase in the loss factor [see Fig. 3(a)], thus entering more and more in the PAM stop band. However, the change in frequency is less than 10% with respect to the lossless case. Figures 3(b) and 3(c) depict the amplitude and the phase of the transmission coefficient of $N = 6$ PAM for different values of the loss factor, respectively. The transmitted amplitude is reduced because of the losses but remains reasonable for the application of zero phase propagation in realistic situations. Moreover, in Fig. 3(d), we represent the dependence of the phase of the transmission coefficient on the number of unit cells considered in the finite length PAM. The variation of the phase remains lower than 8% at $f_{\phi=0}$ in the cases $N \leq 6$.

In order to validate the previous results, we followed a twofold procedure focusing the analysis on the case of $N = 6$ PAM. The first procedure consists in performing full-wave numerical simulations in a 2D-axisymmetric configuration using FEM. The system is insonified by a plane incident wave from left to right, and the plates are composed of viscoelastic material of the above-mentioned properties. A plane wave radiation condition is applied at the waveguide end boundary to avoid spurious reflections. The second procedure is the measurement of the scattering parameters and the recovery of the effective dynamic mass density of the system using the experimental setup shown in Fig. 1(d). The details on the retrieval procedure can be found in Ref. 32 and in supplementary material (S.II).

The red dashed line and symbols in Figs. 3(a)–3(d) show the full numerical and experimental validation of the analytical predictions for

$N = 6$ PAM, respectively. Figure 3(b) depicts the amplitude of the transmission coefficient of the system. A maximum of the transmission coefficient occurs at $f_m = 439$ Hz due to the quasi-impedance matching condition. The phase of the transmission coefficient is shown in Figs. 3(c) and 3(d). A zero phase propagation is measured at $f_{\phi=0} = 389$ Hz, in agreement with the predictions, thus experimentally confirming the feasibility of zero-phase propagation. Good agreement is observed between the measurement, the analytical, and the numerical results.

Figure 4 depicts the real and imaginary parts of the effective dynamic mass density. In the propagative regime, the real part of the effective dynamic mass density is positive, while its imaginary counterpart is negative, thus fulfilling the causality principle. In contrast, both real and imaginary parts of the density are negative in the forbidden bandgap. Moreover, the real and imaginary parts of the density are of the same order of magnitude over the frequency range of interest, contrary to the bulk modulus, the imaginary part of which is much smaller than its real part (see supplementary material Fig. S1). Thus, most of the losses can be attributed to the complex effective mass density. Fairly good agreement is found between the measurement, the numerical, and the analytical predictions. The visible discrepancies are attributed to a residual variability on the unit cells, due to either the clamping condition or the intrinsic properties of the plate. This variability mainly affects the reflection coefficient [see supplementary material (S.IV)] and therefore the effective density.

As an example of application, this peculiar zero phase propagation property is used to create a subwavelength dipole source by considering two waveguides: the first waveguide is filled with a DNZ PAM and the other one is a coiled-up Fabry–Pérot resonator (FPR) occupied by a porous material in order to compensate the amplitude decrease due to the losses of the PAM in the first waveguide. A dipole source can be approximated by two out-of-phase monopoles of equal flow rates, resulting in two symmetric lobes in the polar directivity pattern. By designing the length of this FPR such that its first resonance coincides with the zero-phase frequency of the PAM, the acoustic fields at both waveguide boundaries are out-of-phase, thus fulfilling the design condition for an acoustic dipole.

Figure 5 shows a 2D full-wave simulation of such a device. Using the previously characterized plastic shim material, an $L = 6$ cm periodic arrangement of 6 square plates of width $w = 2$ cm and thickness $h = 102\,\mu$m is tested. The zero-phase frequency of the plate

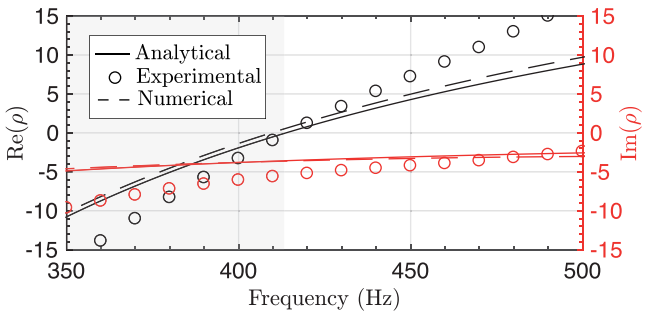

FIG. 4. Analysis of the lossy effective dynamic mass density: real part (black color, left axis) and imaginary part (red color, right axis). Continuous lines, dashed lines, and symbols represent the analytical, numerical, and experimental results, respectively.

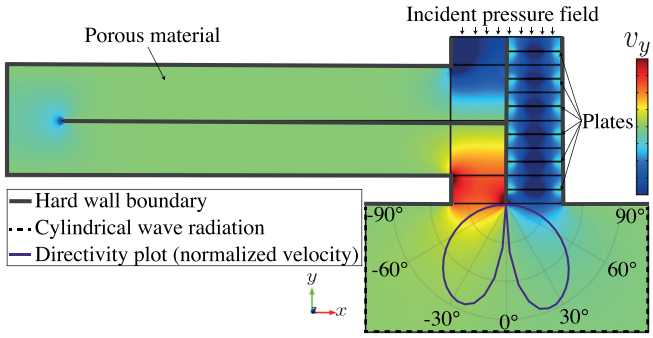

FIG. 5. 2D Full-wave simulation of a subwavelength dipole device built of a coiled-up Fabry–Pérot waveguide of length $L_{FP} \approx 35$ cm and a 6 plates PAM. The y component of the velocity field is shown as well as the normalized directivity polar plot of the dipole (purple line).

lattice is $f_{\phi=0} = 488$ Hz. The 2 cm wide FPR waveguide length is thus $L_{FP} = c_0/(2f_{\phi=0}) \approx 35$ cm long to resonate at that frequency. In the simulation, the FPR is coiled-up to reduce the device total volume (total width: 19.7 cm and total height: 6 cm). To reproduce the sound attenuation of the PAM, the Fabry–Pérot waveguide is filled with a porous medium (porosity: 0.96, flow resistivity: 2847 Pa s m^{-2}, viscous length: 273 μm, thermal length: 672 μm, tortuosity: 1.07, and Biot frequency: $f_c = 334$ Hz)[33–35] lying in the inertial regime at $f_{\phi=0}$. Both waveguides are excited by a plane wave pressure field at the top boundary and radiate in a semi-infinite domain. An out-of-phase equal mean flow rate is found at each outer boundary, leading to a two lobe directivity pattern (purple line) and thus evidencing the efficiency of the device as a subwavelength dipole ($L_x \approx \lambda/4$ for the width and $L_y \approx \lambda/12$ for the height).

In this work, we have reported the impact of the viscothermal and viscoelastic losses on the zero phase propagation regime of a PAM. We have shown that the zero phase propagation appears at frequencies in the negative mass density regime. In this regime, corresponding to the bandgap, the amplitude of the transmission coefficient depends on the number of unit cells in the system. In contrast, the phase of the transmission coefficient remains constant in the lossless case. Therefore, a compromise between the number of unit cells and the variation of the amplitude should be reached. In this case, we consider systems made of $N \leq 6$, leading to a lossless transmission amplitude of $|T| \geq 0.9$. Once the losses are introduced in the system, a weak dependence of both the zero phase frequency, $f_{\phi=0}$, and the phase of the transmission coefficient, ϕ, on both the number of unit cells and the amount of losses is observed. In both cases, the variation is less than 10%. These analytical results have been numerically reproduced by full-wave simulations and experimentally validated by measuring the scattering parameters of a PAM made of $N = 6$ plates as well as the effective mass density. The agreement between the analytical predictions, the numerical simulations, and the experimental results is found to be very good. The results shown in this work pave the way for designing devices based on PAM with zero phase propagation. As an example, a subwavelength acoustic dipole has been designed numerically.

See the supplementary material for the details on the transfer matrix analytical model (S.I); the experimental reconstruction of the

scattering parameters (S.II); the plate characterization process (S.III); the measured scattering parameters and effective dynamic mass density of a 6 PAM (S.IV); and the theoretical reason for the frequency offset between the zero-phase, zero-density, and unit transmission in the case of a noninfinite effective bulk modulus system (S.V).

This article is based upon work from COST Action DENORMS CA15125, supported by COST (European Cooperation in Science and Technology). This work was funded by the Metaroom Project No. ANR-18-CE08-0021 and co-funded by ANR and RCG. J. Christensen acknowledges the support from the MINECO through a Ramón y Cajal grant (Grant No. RYC-2015-17156). J. Sánchez-Dehesa acknowledges the support from the Ministerio de Economía y Competitividad of the Spanish government and the European Union Fondo Europeo de Desarrollo Regional (FEDER) through Project No. TEC2014-53088-C3-1-R.

REFERENCES

[1]S. A. Cummer, J. Christensen, and A. Alù, "Controlling sound with acoustic metamaterials," Nat. Rev. Mater. **1**, 16001 (2016).
[2]G. Ma and P. Sheng, "Acoustic metamaterials: From local resonances to broad horizons," Sci. Adv. **2**, e1501595 (2016).
[3]M. Yang and P. Sheng, "Sound absorption structures: From porous media to acoustic metamaterials," Annu. Rev. Mater. Res. **47**, 83–114 (2017).
[4]P. A. Deymier, *Acoustic Metamaterials and Phononic Crystals*, Springer Series in Solid-State Sciences Vol. 173 (Springer-Verlag, Berlin/Heidelberg, 2013).
[5]Z. Liu, X. Zhang, Y. Mao, Y. Y. Zhu, Z. Yang, C. T. Chan, and P. Sheng, "Locally resonant sonic materials," Science **289**, 1734–1736 (2000).
[6]P. Sheng, X. X. Zhang, Z. Liu, and C. T. Chan, "Locally resonant sonic materials," Physica B **338**, 201–205 (2003).
[7]Z. Yang, J. Mei, M. Yang, N. H. Chan, and P. Sheng, "Membrane-type acoustic metamaterial with negative dynamic mass," Phys. Rev. Lett. **101**, 204301 (2008).
[8]C. M. Park, J. J. Park, S. H. Lee, Y. M. Seo, C. K. Kim, and S. H. Lee, "Amplification of acoustic evanescent waves using metamaterial slabs," Phys. Rev. Lett. **107**, 194301 (2011).
[9]A. Alù, M. G. Silveirinha, and N. Engheta, "Transmission-line analysis of ϵ-near-zero–filled narrow channels," Phys. Rev. E **78**, 016604 (2008).
[10]B. Edwards, A. Alù, M. E. Young, M. Silveirinha, and N. Engheta, "Experimental verification of epsilon-near-zero metamaterial coupling and energy squeezing using a microwave waveguide," Phys. Rev. Lett. **100**, 033903 (2008).
[11]J. J. Park, K. J. B. Lee, O. B. Wright, M. K. Jung, and S. H. Lee, "Giant acoustic concentration by extraordinary transmission in zero-mass metamaterials," Phys. Rev. Lett. **110**, 244302 (2013).
[12]A. Alù, M. G. Silveirinha, A. Salandrino, and N. Engheta, "Epsilon-near-zero metamaterials and electromagnetic sources: Tailoring the radiation phase pattern," Phys. Rev. B **75**, 155410 (2007).
[13]M. Silveirinha and N. Engheta, "Tunneling of electromagnetic energy through subwavelength channels and bends using ϵ-near-zero materials," Phys. Rev. Lett. **97**, 157403 (2006).
[14]M. G. Silveirinha and N. Engheta, "Theory of supercoupling, squeezing wave energy, and field confinement in narrow channels and tight bends using ϵ near-zero metamaterials," Phys. Rev. B **76**, 245109 (2007).
[15]R. Liu, Q. Cheng, T. Hand, J. J. Mock, T. J. Cui, S. A. Cummer, and D. R. Smith, "Experimental demonstration of electromagnetic tunneling through an epsilon-near-zero metamaterial at microwave frequencies," Phys. Rev. Lett. **100**, 023903 (2008).
[16]B. Edwards, A. Al, M. G. Silveirinha, and N. Engheta, "Reflectionless sharp bends and corners in waveguides using epsilon-near-zero effects," J. Appl. Phys. **105**, 044905 (2009).
[17]R. Fleury and A. Alù, "Extraordinary sound transmission through density-near-zero ultranarrow channels," Phys. Rev. Lett. **111**, 055501 (2013).
[18]R. Graciá-Salgado, V. M. García-Chocano, D. Torrent, and J. Sánchez-Dehesa, "Negative mass density and ρ-near-zero quasi-two-dimensional metamaterials: Design and applications," Phys. Rev. B **88**, 224305 (2013).
[19]A. Alù and N. Engheta, "Coaxial-to-waveguide matching with ε-near-zero ultranarrow channels and bends," IEEE Trans. Antennas Propag. **58**, 328–339 (2010).
[20]A. Alù and N. Engheta, "Light squeezing through arbitrarily shaped plasmonic channels and sharp bends," Phys. Rev. B **78**, 035440 (2008).
[21]A. Alù and N. Engheta, "Dielectric sensing in ϵ-near-zero narrow waveguide channels," Phys. Rev. B **78**, 045102 (2008).
[22]D. A. Powell, A. Alù, B. Edwards, A. Vakil, Y. S. Kivshar, and N. Engheta, "Nonlinear control of tunneling through an epsilon-near-zero channel," Phys. Rev. B **79**, 245135 (2009).
[23]C. Argyropoulos, P.-Y. Chen, G. D'Aguanno, N. Engheta, and A. Alù, "Boosting optical nonlinearities in ϵ-near-zero plasmonic channels," Phys. Rev. B **85**, 045129 (2012).
[24]R. W. Ziolkowski, "Propagation in and scattering from a matched metamaterial having a zero index of refraction," Phys. Rev. E **70**, 046608 (2004).
[25]F. Bongard, H. Lissek, and J. R. Mosig, "Acoustic transmission line metamaterial with negative/zero/positive refractive index," Phys. Rev. B **82**, 094306 (2010).
[26]T.-Y. Huang, C. Shen, and Y. Jing, "Membrane- and plate-type acoustic metamaterials," J. Acoust. Soc. Am. **139**, 3240–3250 (2016).
[27]G. Ma, M. Yang, S. Xiao, Z. Yang, and P. Sheng, "Acoustic metasurface with hybrid resonances," Nat. Mater. **13**, 873–878 (2014).
[28]V. Romero-García, G. Theocharis, O. Richoux, A. Merkel, V. Tournat, and V. Pagneux, "Perfect and broadband acoustic absorption by critically coupled sub-wavelength resonators," Sci. Rep. **6**, 19519 (2016).
[29]V. Cutanda Henriquez, V. Garcia-Chocano, and J. Sanchez-Dehesa, "Viscothermal losses in double-negative acoustic metamaterials," Phys. Rev. Appl. **8**, 014029 (2017).
[30]C. Zwikker and C. W. Kosten, "Sound absorbing materials," (1949).
[31]M. R. Stinson, "The propagation of plane sound waves in narrow and wide circular tubes, and generalization to uniform tubes of arbitrary cross-sectional shape," J. Acoust. Soc. Am. **89**, 550 (1991).
[32]M. Niskanen, J. Groby, A. Duclos, O. Dazel, J. C. Le Roux, N. Poulain, T. Huttunen, and T. Lähivaara, "Deterministic and statistical characterization of rigid frame porous materials from impedance tube measurements," J. Acoust. Soc. Am. **142**, 2407 (2017).
[33]J.-P. Groby, W. Lauriks, and T. E. Vigran, "Total absorption peak by use of a rigid frame porous layer backed by a rigid multi-irregularities grating," J. Acoust. Soc. Am. **127**, 2865–2874 (2010).
[34]J.-F. Allard and N. Atalla, *Propagation of Sound in Porous Media: Modelling Sound Absorbing Materials* (Wiley-Blackwell, 2009).
[35]L. De Ryck, J.-P. Groby, P. Leclaire, W. Lauriks, A. Wirgin, Z. E. A. Fellah, and C. Depollier, "Acoustic wave propagation in a macroscopically inhomogeneous porous medium saturated by a fluid," Appl. Phys. Lett. **90**, 181901 (2007).